scientific reports

OPEN

Sealing mechanisms and enrichment patterns of deep coalbed methane: insights from the Jiaxian block, Ordos Basin

Qifan Zhang[1,2,3], Peijie Li[4], Dameng Liu[1,2,3 ✉], Yanbin Yao[1,2,3], Yidong Cai[1,2,3], Yilin Guo[1,2,3] & Zefan Wang[1,2,3]

The enrichment of deep coalbed methane (CBM) in the Jiaxian block of the Ordos Basin is strongly influenced by the sealing capacity of coal seam roofs and floors, which play a pivotal role in CBM preservation under conditions of high temperature and pressure. Despite its importance, the mechanisms underlying the sealing capacity remain poorly understood, and their quantitative evaluation is rarely explored. This study starts from the influence of gas transport channels, and summarizes the key factors that affect sealing capability. And it addresses these gaps by integrating experimental methods, advanced 3D seismic attribute analysis, and multi-source data fusion to construct a comprehensive model for evaluating roof and floor sealing capacity. Our findings reveal that five key factors—mud content, mudstone-to-formation ratio, porosity, permeability, and fracture development intensity—control the sealing capacity of the roof and floor. Focusing on the No. 8 coal seam, we developed a novel methodology to predict porosity and permeability by differentiating rock types, coupled with fracture intensity prediction using optimized seismic attributes and grayscale calculations. The results provide crucial insights into the enrichment patterns of deep CBM, offering a novel framework for optimizing exploration strategies in the Ordos Basin and beyond.

Deep coalbed methane (CBM) resources in China are substantial; the buried depth of 1500–3000 m of deep CBM resources is approximately 30.37×10^{12} m^3, which is twice as much as the shallow CBM resources at depths of < 1500 m[1]. Deep CBM resources constitute an important part of China's overall CBM resources[2]. Since 2019, the Daning–Jixian block on the eastern margin of the Ordos Basin has gradually entered the stage of large-scale delineation exploration for deep CBM, with a daily gas production of vertical wells exceeding 2×10^4 m^3 and that of horizontal wells exceeding 10×10^4 m^3. This represents a major breakthrough in deep CBM exploration and development[3]. The Jiaxian block is situated in the northeast sector of the Ordos Basin, where the No. 8 coal seam of the Benxi Formation is buried at a depth of > 2000 m, indicating significant resource potential[4]. The proportion of free gas in deep CBM is relatively high under high temperature and high pressure. The sealing effect of the roof and floor on free gas has a significant impact on the total gas content[5]. Currently, the study area is in the early stages of deep CBM exploration, and theoretical research on the exploration and development of CBM at depths of > 2000 m remains in its infancy, with key issues such as preservation conditions and enrichment rules of deep CBM remaining unclear.

Studies by Qin et al. demonstrated that the genesis of CBM involves biogenic as well as thermal processes. If the sealing capacity of the roof is poor, the secondary biogenic gas generated in the middle and later stages of the coal reservoir can easily escape[6]. Therefore, the sealing capacities of the roof and floor of coal seams are important factors affecting the preservation conditions and enrichment degree of CBM[7-9]. Meng et al. concluded that the sealing capacity of the roof is closely related to its lithology and physical properties, but they only characterized the relationship between lithology and gas content[10]. Jin et al. concluded that the lithology of the roof has a significant influence on the preservation of CBM and described the physical characteristics of various types of

[1]School of Energy Resources, China University of Geosciences, Beijing 100083, China. [2]Coal Reservoir Laboratory of National Engineering Research Center of CBM Development & Utilization, China University of Geosciences, Beijing 100083, China. [3]Frontiers Science Center for Deep-time Digital Earth, China University of Geosciences, Beijing 100083, China. [4]PetroChina Jidong Oilfield Company, Tangshan 063000, China. ✉email: dmliu@cugb.edu.cn

lithology but did not reach a clear conclusion[11]. The previous evaluation of the roof sealing ability was only a qualitative description of a small amount of experimental data, lacking quantitative evaluation, and had little practical application value. Liu et al. conducted a theoretical study on the evaluation model of sealing capacities for the roof and floor using geophysical logging data, but no experimental data were available to further validate their findings[12]. Tian et al. used experimental methods and simulations to discuss the relationship between the escape amount of CBM and the sealing capacity of different lithological roof. However, they only considered the sealing ability of a single lithology, lacking comprehensive consideration of the actual lithological combinations present in the formations[13]. The actual strata are heterogeneous, which is composed of rocks of different thicknesses. It is not meaningful to discuss the sealing ability of a certain lithology separately. It is necessary to combine the sealing ability of a single lithology with the actual strata to evaluate the comprehensive sealing ability of a certain thickness of strata. Moreover, the experimental data in the research area is limited, and a comprehensive evaluation needs to be conducted by combining well logging and seismic data for evaluation.

The factors affecting the sealing capacity are complex, but the sealing capacity of geological formations is mainly about free gas in free state, which is essentially related to the scale and connectivity of migration channels. The pores, microcracks, and various forms of micro permeable spaces in the roof and floor provide channels for gas to escape. Therefore, it is necessary to comprehensively analyze the influencing factors of the migration channels from both micro and macro perspectives to evaluate the sealing ability of the roof and floor.

This study focuses on the roof and floor of the No. 8 coal seam and explores the logging information in depth, integrating drilling and physical experimental data to evaluate the physical properties and fracture development characteristics, five parameters that effectively reflect sealing capacities were identified: mud content, mudstone-to-formation ratio, porosity, permeability, and fracture development intensity. A comprehensive calculation model was subsequently constructed to evaluate the sealing capacities of the roof and floor of the coal seams quantitatively. Moreover, the influence of the roof and floor on deep CBM accumulation was analyzed.

Geological background

The Ordos Basin comprises six primary tectonic units: the Jinxi Flexure Belt to the east, the Weibei Uplift Belt to the south, the Yimeng Uplift Belt to the north, the Tianhuan Depression to the west, the northern slope belt in the central part of Shaanxi Province, and the Western Marginal Alluvial Belt. The tectonic evolution of the basin has progressed through several stages, including the formation of the crystalline basement of the platform, a period of stable platform development, and the formation and evolution of the basin's tectonic pattern characterized by uplift and depression[14]. Notably, the Yanshan and Himalayan movements during the Middle Cenozoic era significantly influenced the tectonic configuration of the Ordos Basin, resulting in a north–south warping, a gradual and elongated eastern flank, and a short and steep western flank. The overall tectonic structure is relatively simple, and the stratigraphy displays a gentle disposition[15]. The study area is located on the Yishan Slope in the northeast sector of the Ordos Basin. The stratigraphy in this area exhibits gently westward monoclinal tectonics, with a dip of less than 2°[16], as illustrated in Fig. 1.

The strata in the Ordos basin include Cambrian, Ordovician, Carboniferous Benxi Formation (C2b), Permian Taiyuan Formation (C3t) and Shanxi Formation (P1s), Xiashihezi Formation (P1x), Shangshihezi Formation (P2s) and Shiqianfeng Formation (P2sh), Triassic Liujiagou Formation (T1l) and Quaternary deposit[17], as shown in Fig. 2. The C2b formation is deposited above the Ordovician formation with an unconformity, and the Quaternary deposit lies above Triassic or Permian formation also with an unconformity. The C2b, C3t, and P1s formations are the primary strata that contain coal. The depositional environment of coal in C2b is continental oceanic interaction environment, and the extensive water-covered environment is conducive to plant growth, thus the coal seam is well developed. Among them, the no. 8 coal seam is characterized by its substantial thickness and advanced stage of maturation, which is currently the main target for deep CBM development in our study area.

Data and methods
### Geophysical logging data

Due to the limitations of core sampling and core analysis testing conditions, using logging data to evaluate the pore parameters of coal seams, roofs, and floors is an economical and efficient method[15]. The sealing capacities of the roof and floor of the No. 8 coal seam were evaluated using geophysical logging data from 67 wells in the study area. The rock samples of the roof and floor were classified according to lithology and multivariate linear fitting with the logging data was performed to optimize the logging curves. Then, based on the optimized logging curves, multiple linear regression is performed to construct logging prediction models for porosity and permeability of different rock types. In addition, the mud content (V_{sh}) was calculated based on natural gamma (GR). Well logging data includes natural gamma, density (DEN), acoustic time difference (AC), compensated neutron (CNL), natural potential (SP), wellbore diameter (CAL), shallow lateral resistivity (RLLS), and deep lateral resistivity (RLLD).

Samples and experiments

Totally 16 samples from the roof and floor of no. 8 coal seam in 4 CBM wells were tested for this study, and their locations are shown in Fig. 1. The samples were carefully packed. Then, porosity and permeability were analyzed.

The porosity was experimented by Poro PDP-200 porosity tester. Porosity test was performed following Standard of the Ministry of Coal Industry of the People's Republic of China MT/T 41-1987 for 16 samples to measure porosity of rocks.

The permeability was experimented by Poro PDP-200 porosity tester. Permeability test was performed following Industry Standards of the People's Republic of China MT/T 223 – 90 for 16 samples. This experiment
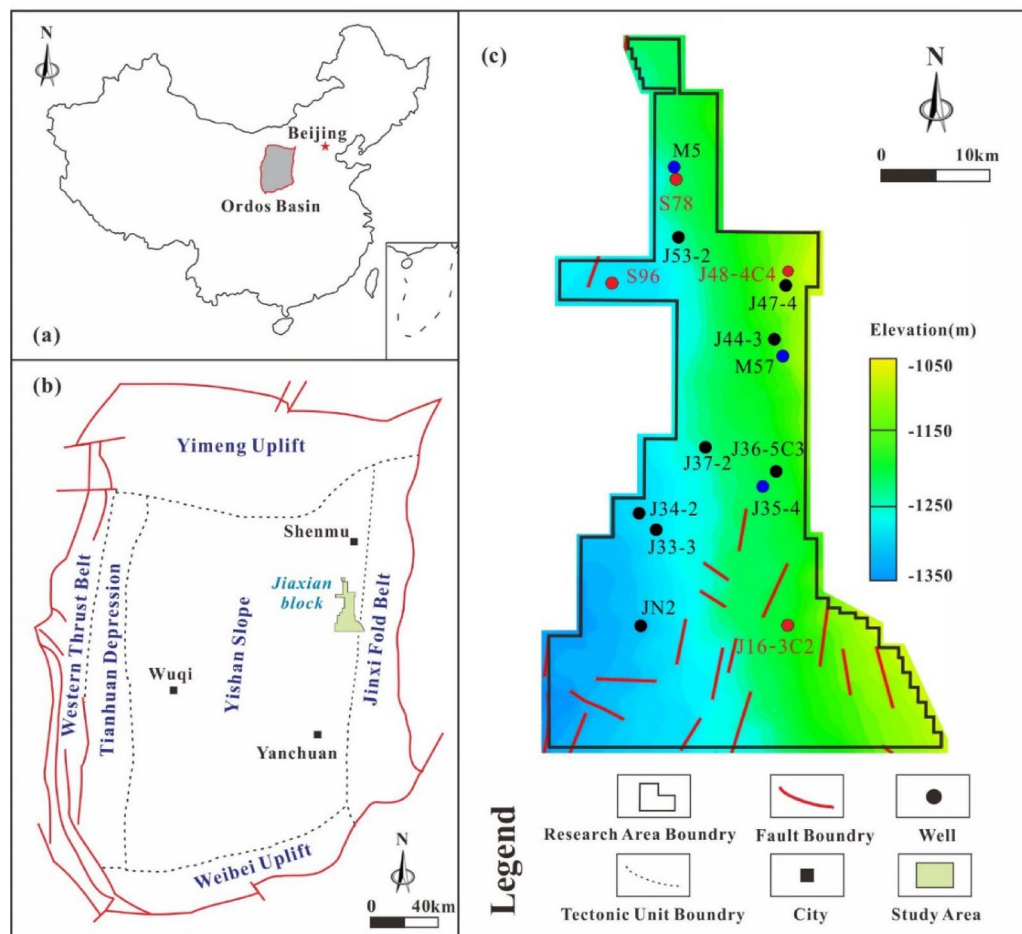
Fig. 1. Locations of Jiaxian block and wells [modified with permission from ref.[4] (Copyright 2024, The Authors, published by *Coal Geology & Exploration*)].

used nitrogen to determine the permeability of rocks. Permeability tests were carried out at a temperature of 30 °C and a pore pressure of 0.5 MPa, using methane as the testing fluid, with the confining pressure varying between 2 and 15 MPa.

RGB fusion technology

RGB (red, green, and blue) fusion technology refers to the use of red, green, and blue to represent a single seismic attribute, and then overlaying the three attributes in color to achieve multi-attribute fusion[18]. Usually, cluster analysis or principal component analysis is used to select three attributes from multiple seismic attributes, and then RGB fusion is performed to generate attribute slices. The values of three primary colors are 0 to 255, so there are 256*256*256 colors can be obtained to represent different features through fusion. The fused seismic attributes can comprehensively reflect common characteristics by highlighting similarities and diminishing differences, and be able to compensate the shortcomings of a single seismic attribute that cannot highlight regional anomalies by highlighting commonalities and weakening differences. Therefore, the fused seismic attributes contain more accurate geological information[19].

Results

Experimental results on porosity and permeability of the roof and floor

Three main rock types of the roof and floor are sandstone, mudstone, and limestone in the study area. The results of porosity and permeability are given in Table 1. The porosity of the sandstone ranges from 0.809 to 11.296%, and the gas permeability ranges from 2.88mD to 7.25mD. The porosity of the mudstone ranges from 0.849 to 1.91%, and the gas permeability ranges from 0.01mD to 2.23mD. And the porosity of the limestone ranges from 0.94 to 2.01%, and the gas permeability ranges from 0.78mD to 3.86mD.

Evaluation parameters affecting sealing capacity

The sealing ability of geological formations to gas depends on the migration channels. Pores, microcracks, and various forms of micro permeable spaces are interconnected to form migration channels. Therefore, we
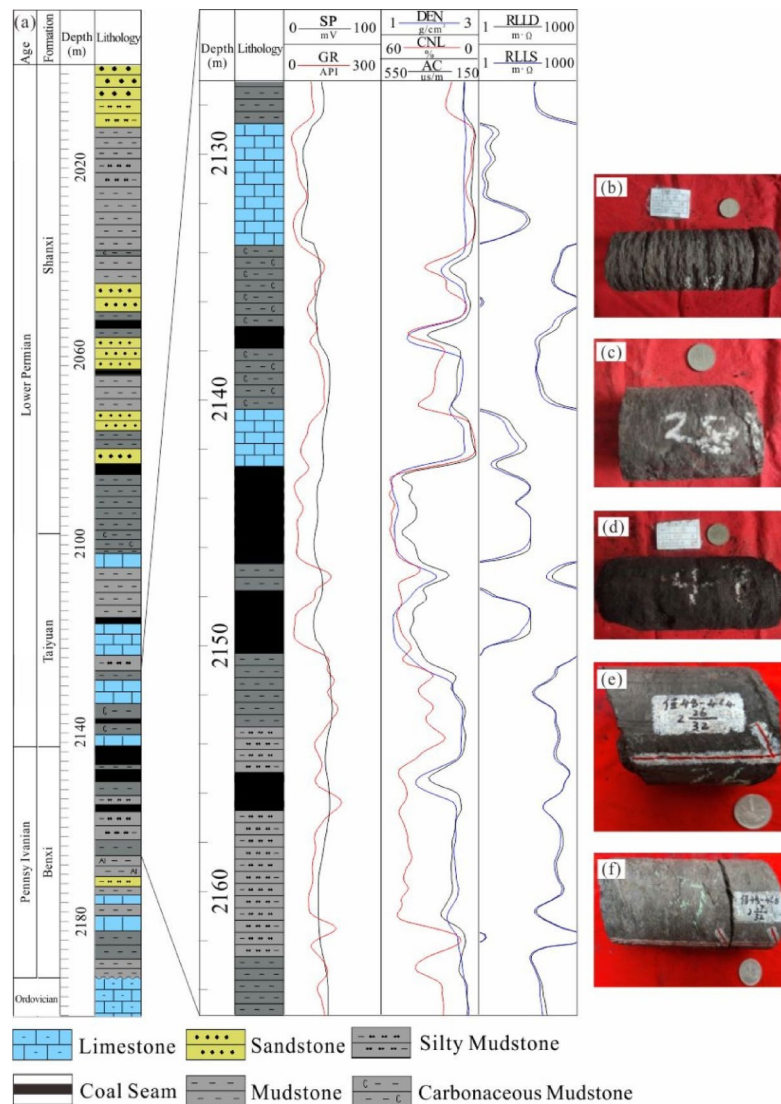
Fig. 2. Stratigraphic column and core photos of coal-bearing sequence. [Modified with permission from ref.[4] (Copyright 2024, The Authors, published by *Coal Geology & Exploration*)]. (**a**) Stratigraphic column of the J16-3C2. (**b**) Dark grey mudstone of the Permian Taiyuan Formation in J16-3C2 at the depth of 2137.7 m. (**c**) Dark grey argillaceous limestone of the Permian Taiyuan Formation in J16-3C2 at the depth of 2140.7 m. (**d**) Black coal of the Carboniferous Benxi Formation in J16-3C2 at the depth of 2143.4 m. (**e**) Dark grey carbonaceous mudstone of the Carboniferous Benxi Formation in J48-4C4 at the depth of 2097.1 m. (**f**) Grey siltstone of the Carboniferous Benxi Formation in J48-4C4 at the depth of 2098.0 m.

comprehensively consider the factors affecting migration channels of the roof and floor from micro to macro levels to analyze their sealing capacities.

Microscopically, the gaps between mineral particles form migration channels. And the smaller the mineral particles, the smaller the channels formed. Among various lithologies in the study area, mudstone has the smallest particle size, which means that the higher the mud content, the smaller the independent migration space formed. The porosity of rocks reflects the proportion of pore space, which can be understood as the sum of all migration spaces. The larger the porosity, the larger the migration space. In addition, channels need to be interconnected for gas to escape, and permeability is an important parameter reflecting pore connectivity. The larger the porosity, the smoother the migration channel, and the poorer the sealing capability. Therefore, mud content, porosity, and permeability are the three important factors that affect the sealing capability microscopically.

Macroscopically, large migration channels such as cracks and faults are also channels for rapid gas migration. In addition, the roof and floor in the study area are mainly composed of sandstone, mudstone, and limestone. As we discussed earlier, mudstone is the densest, so the higher the ratio of mudstone to formation, the stronger the overall sealing capability of the formation. But when considering this issue, it is also important to note that the distance between mudstone and coal seam in the combination will greatly affect its sealing ability. It should also be noted that the distance between mudstone and coal seams in the combination significantly impacts its sealing

Well	Samples	Lithology	Porosity (%)	Permeability (mD)
S78	Z1-78	Siltstone	1.813	2.880
	Z2-78	Carbonaceous mudstone	0.849	0.010
	Z3-78	Argillaceous siltstone	0.809	3.540
	Z4-78	Carbonaceous mudstone	1.087	0.610
S96	Z1-96	Coarse sandstone	6.435	7.250
	Z2-96	Mudstone	1.149	2.230
	Z3-96	Sandstone	11.296	4.320
J48-4C4	Z1-4-48	Carbonaceous mudstone	1.300	0.162
J16-3C2	Z1-3-16	Mudstone	1.910	1.260
	Z2-3-16	Mudstone	1.630	1.120
	Z3-3-16	Mudstone	1.630	1.590
	Z4-3-16	Argillaceous limestone	0.940	0.850
	Z5-3-16	Argillaceous limestone	1.160	0.780
	Z6-3-16	Argillaceous limestone	1.550	3.860
	Z7-3-16	Argillaceous limestone	2.010	3.750
	Z8-3-16	Argillaceous limestone	1.600	2.250

Table 1. Porosity and permeability of the roof and floor.
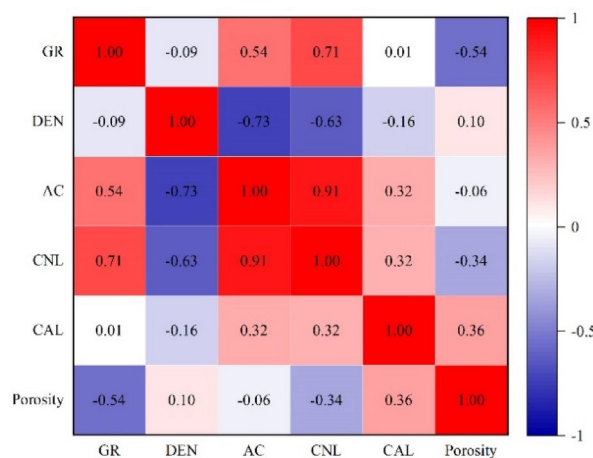
Fig. 3. Pearson correlation between porosity and logging curves.

capacity. The smaller the distance, the stronger the influence of mudstone. Therefore, the development intensity of fracture and the mudstone to formation ratio are two macro factors that affect the sealing capacity. And the distance index also has an impact on the sealing capability.

Five parameters effectively reflect the sealing capacity, including mud content, mudstone-to-formation ratio, porosity, permeability, and fracture development intensity. Experimental data for determining these parameter values are scarce as most study areas only include experimental measurements from selected sections of typical wells. Owing to the limited experimental data, it is necessary to utilize geophysical logging data and seismic data to estimate the evaluation parameters for sealing capacity. Different logging data can reflect various physical properties, and parameters can be predicted based on logging curves. By analyzing the correlation between geophysical data and experimental data on the physical properties of the roof and floor in the study area, models were established to estimate these physical properties. Additionally, different attributes were extracted from 3D seismic data based on their physical significance, corresponding to the characteristics of the desired parameters. This approach allows for the prediction of evaluation parameters at all 67 wells in the study area, using experimental data from four wells. Furthermore, seismic data can be extended to any point within the study area. This method can significantly enhance the understanding of the spatial distribution of sealing capacity in the roof and floor of the study area.

Logging prediction for physical properties of different lithologies
Logging prediction of porosity
Sediments of varying grain sizes form channels of different dimensions and exhibit different sealing effects on gas. The DEN, AC, CAL, and CNL logging curves that show a higher correlation with porosity were selected using the Pearson correlation coefficient, as illustrated in Fig. 3. Porosity is influenced by sediment type; therefore, it

is not feasible to use logging data to uniformly predict physical property parameters. After classifying the roof and floor rock samples by lithology, they were multivariate linear fitted with logging data separately, as shown in Fig. 4. It was observed that the porosity of sandstone correlates well with DEN and CNL but shows a poor correlation with the other logging curves. Consequently, the porosity of the sandstone can be estimated based on multiple linear regression of DEN and CNL, as shown in Eq. 1 with R2 = 0.98. Estimating porosity prediction formulas for limestone and mudstone similarly is presented in Eq. 2 and Eq. 3.

$$\varphi_S = -40.01\text{DEN} - 0.08\text{CNL} + 110.36 \tag{1}$$

$$\varphi_L = -62.14\text{DEN} + 0.01\text{AC} - 2.82\text{CNL} + 174.49 \tag{2}$$

$$\varphi_M = 1.39\text{DEN} + 0.04\text{CNL} - 0.09\text{CAL} - 1.46 \tag{3}$$

Where φ_S, φ_L, φ_M respectively stand for porosities of sandstone, limestone and mudstone, %.

Logging prediction of permeability
Using the same method to predict the permeability of the roof and floor. Select the DEN, GR, CAL, and CNL logging data that exhibit a higher correlation with permeability using the Pearson correlation coefficient, as shown in Fig. 5. Fit the permeability of the samples to the logging data, as shown in Fig. 6. The permeability of different lithology can be estimated by Eq. 4, Eq. 5 and Eq. 6. Notably, the permeability of limestone correlates well with DEN, GR, CAL, and CNL. Notably, the permeability of limestone correlates well with DEN, GR, CAL, and CNL. However, the DEN and CAL values are not indicative due to their minimal differences. Consequently, GR and CNL were used to construct a multivariate linear model for limestone permeability.

$$K_S = 5.71\text{CAL} + 0.05\text{CNL} - 122.14 \tag{4}$$

$$K_L = -0.08\text{GR} + 0.38\text{CNL} + 4.33 \tag{5}$$

$$K_M = 0.032\text{CNL} - 0.02\text{GR} + 2.85 \tag{6}$$

Where K_S, K_L, K_M respectively stand for permeabilities of sandstone, limestone and mudstone, %.
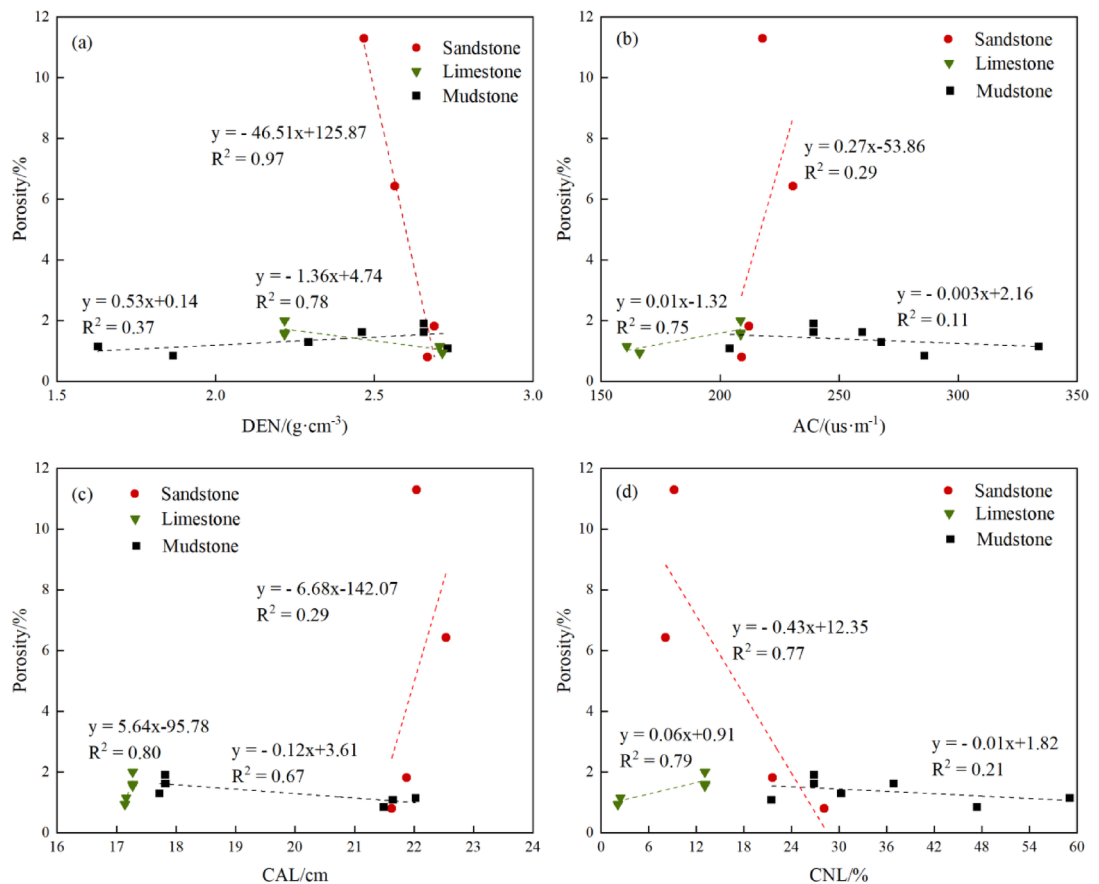
Fig. 4. Linear correlation analysis between porosity and logging curves. (**a**) The correlation between porosity and DEN. (**b**) The correlation between porosity and AC. (**c**) The correlation between porosity and CAL. (**d**) The correlation between porosity and CNL.
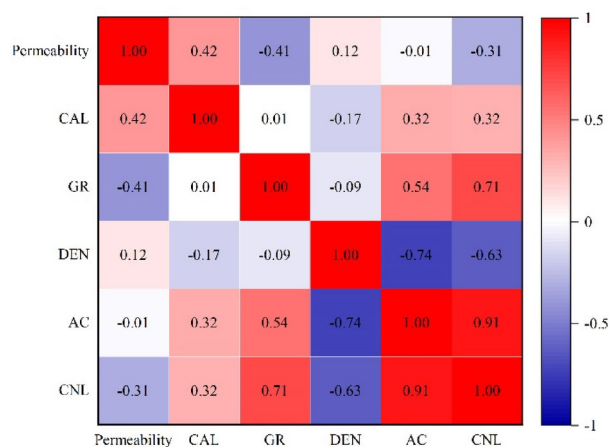
Fig. 5. Pearson correlation between permeability and logging curves.
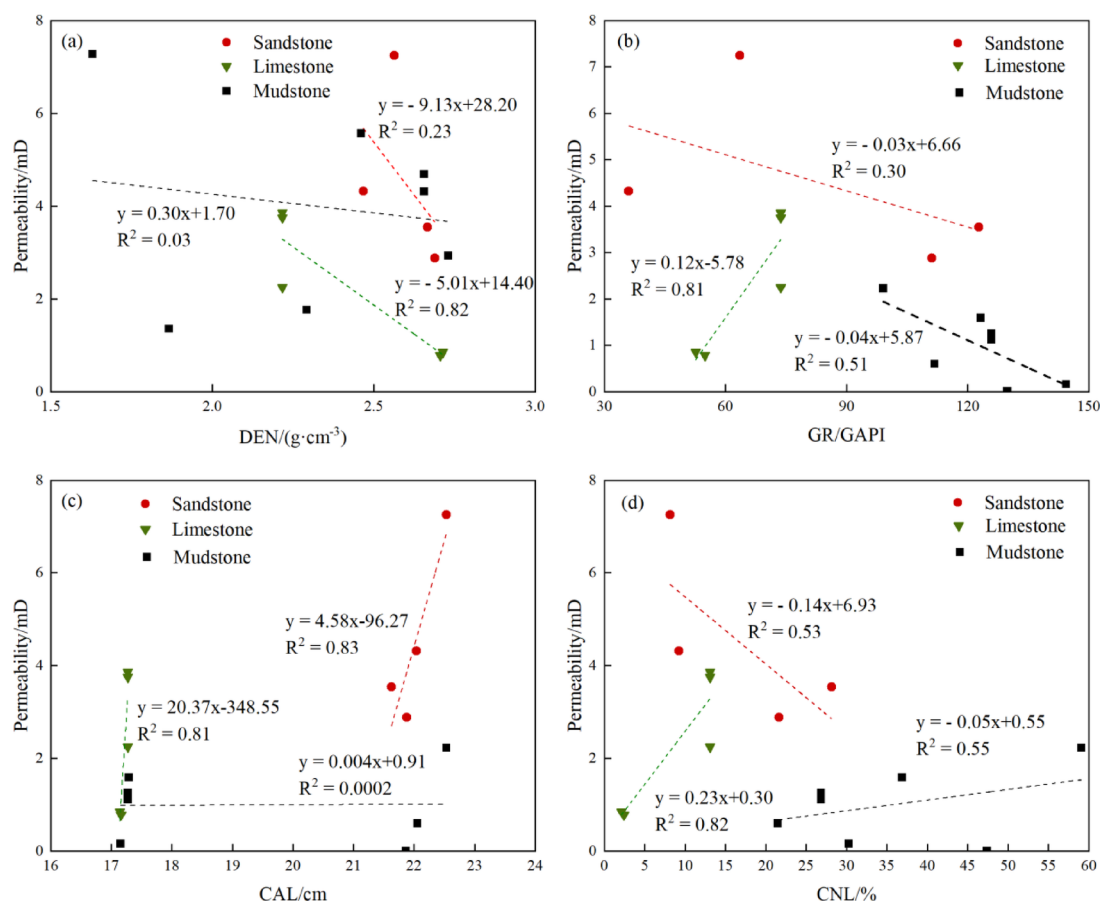
Fig. 6. Linear correlation analysis between permeability and logging curves. (**a**) The correlation between permeability and DEN. (**b**) The correlation between permeability and AC. (**c**) The correlation between permeability and CAL. (**d**) The correlation between permeability and CNL.

Determination methods of fracture development intensity

Logging data can only characterize the intensity of fracture development at a specific point, and it is difficult to accurately represent this intensity in most other areas. Therefore, using 3D seismic data to predict fracture development intensity is more effective. Based on seismic data, seismic attributes were extracted to indicate fractures. Seismic attributes refer to the geometric, dynamic, kinematic, and statistical characteristics of seismic waves calculated from seismic data, including curvature, coherence, dip, etc. Curvature refers to the degree of the curvature of a surface. The development of cracks induces positive curvature upward tilt and negative

curvature downward tilt. Therefore, curvature properties can be used to indicate cracks[20,21]. Coherence indicates changes in seismic data related to continuity variations between adjacent traces[22]. Similarity expresses the degree of similarity between two or more seismic traces, considering the amplitude difference between them[23]. Local variability refers to the degree of elevation change of a layer at a specific point compared with surrounding points, which can reflect whether there is a sudden change. Dip refers to the angle between the maximum inclination line of the formation and the horizontal plane, which can indicate minor changes in the formation[24]. The instantaneous phase at the sample location emphasizes the spatial continuity of reflections by providing a way for weak and robust events to appear with equal strength[25].

Fracture-sensitive seismic attribute optimization
Taking the roof as an example, we extract the curvature, coherence, similarity, and dip attributes that may significantly respond to faults in the roof for optimal selection[26]. We filter the attribute values at the fault location and compare the filtered attribute values with all attribute values on the attribute plane using a histogram of the flat distribution (Fig. 7).

It was observed that for the curvature attribute, the distribution of attribute values at the fault location and the overall attribute values fell within the range of 0–0.3. However, the principal frequencies differ, with the curvature attribute values at the fault location ranging from 0.1 to 0.15, while the overall curvature attribute values span from 0 to 0.05. This evidence indicates that the attribute values at the fault deviate more significantly from the characteristics of the attribute values in the entire region, suggesting that the curvature attribute serves as a significant indicator of faults.

Additionally, for the dip attribute, the values at the fault location and the overall values were within the range of 0–2.4. However, the principal frequencies differ: at the fault location, the principal frequency was between 0.8 and 1, whereas the principal frequency for the overall dip attribute values ranged from 0.4 to 0.6. Similarly, for the instantaneous phase attribute, both the fault location and overall attribute values were generally within the range of −140 to 100. The principal frequencies, however, differed, with the fault location having a principal frequency between −80 and −40, while the overall principal frequency ranged from −40 to 0. This indicates that the dip and instantaneous phase attributes also serve as effective indicators of faults.

By contrast, for the coherence attribute, the distribution range of values at the fault location is similar to that of the overall attribute values, and the principal frequency remains the same. This finding suggests that the coherence does not have a significant effect on fault indication. Likewise, the similarity and local variability are not effective indicators of faults. In conclusion, the curvature, dip, and instantaneous phase attributes are selected to characterize the intensity of fracture development, denoted as F.

Seismic attribute fusion for fracture characterization
Fuse the optimized seismic attributes using RGB fusion technology, integrating the responses of curvature, dip, and instantaneous phase attributes to more comprehensively reflect fractures. Utilize the fused seismic attributes to indicate the intensity of fracture development, as shown in Fig. 8.

Due to the fact that RGB attribute fusion technology is a seismic attribute display method, the fused attribute is essentially three-dimensional data represented in different colors. Therefore, the fused attribute values are converted into grayscale values to characterize the strength of fracture development[27].

$$Gray\,(x,y) = R\,(x,y) * 0.299 + G\,(x,y) * 0.587 + B\,(x,y) * 0.114 \tag{7}$$

The characterization effect of the fused attributes was verified via RGB fusion technology using imaging logging data. In fractured formations, mud intrusion into the fractures causes the resistivity and acoustic impedance of fractured reservoirs to be significantly lower than those of the surrounding rocks, resulting in dark stripes on the imaging map[28,29]. Therefore, imaging logging data can be utilized for fracture identification and fracture development analysis. The imaging logging data from eight wells in the study area reflect the strength of fracture development in the roof and floor at their respective locations (Fig. 9), with their locations indicated in Fig. 1. Specifically, fractures are present in the roof of J33-3 and the floor of J36-5C3 and JN2, while no fractures are found in the other wells. Comparing this with the fused attributes of the roof and floor at the corresponding positions, as shown in Table 2, it was found that the fused attribute values are relatively high at locations of fracture development, indicating that the fused attribute has a predictive effect on fractures.

Eventually, a comprehensive evaluation index calculation model for sealing capacities was constructed by selecting five parameters that effectively reflect the sealing capacities: mud content, mudstone-to-formation ratio, porosity, permeability, and fracture development intensity.

Discussion
Sealing capacity evaluation model
Due to the large specific surface area of mud particles, they have strong adsorption capacity for radioactive substances, and GR logging records the intensity of radioactive elements in the rock. Therefore, the mud content (V_{sh}) can be calculated based on GR. The mud content derived from GR is expressed as:

$$V_{sh} = \frac{2^{GCUR \cdot I_{GR}} - 1}{2^{GCUR} - 1} \tag{8}$$

Where V_{sh} is mud content, %; GCUR is Hilchie index related to geological age of strata, generally, GCUR = 3.7 in Paleogene-Neogene strata and GCUR = 2 in older strata; I_{GR} is natural gamma relative value, %.
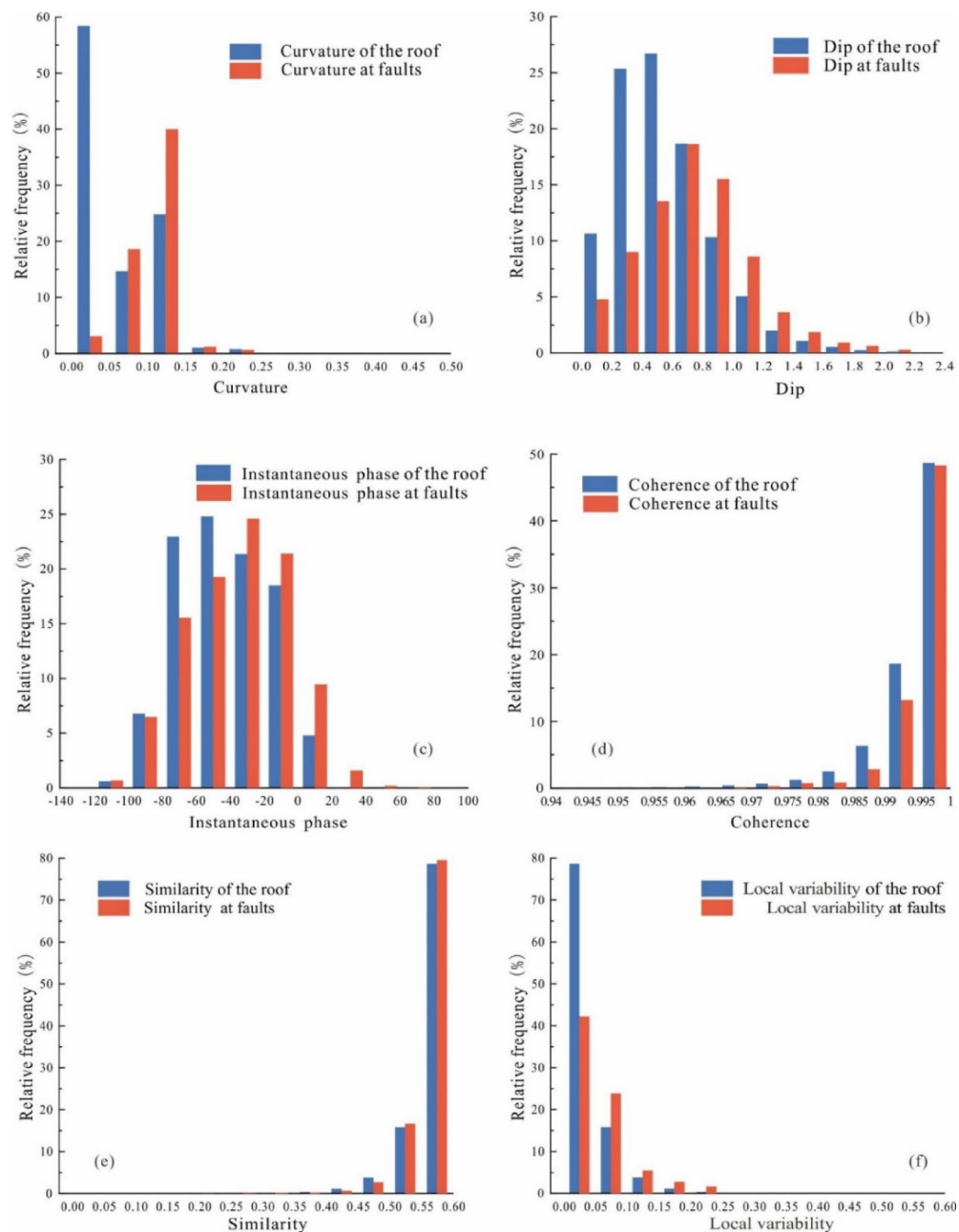
Fig. 7. Comparison between the attributes at the faults and attributes of the roof. (**a**) Comparison between the curvature at the faults and curvature of the roof. (**b**) Comparison between the dip at the faults and dip of the roof. (**c**) Comparison between the instantaneous phase at the faults and similarity of the roof. (**d**) Comparison between the coherence at the faults and coherence of the roof. (**e**) Comparison between the similarity at the faults and similarity of the roof. (**f**) Comparison between the degree of local variability at the faults and degree of local variability of the roof.

Due to the fact that the roof and floor are composed of rocks of different thicknesses, it is not sufficient to simply consider the thickness of a single lithology. Therefore, we have chosen the strata within 15 m above the coal seam as the roof, and the same applies to the floor. No matter what lithological combination, it is sufficient to preserve CBM at this thickness[12]. The roof and floor comprise multiple single layers, each measuring 0.125 m, with the same sampling interval as that of the logging data. Using logging data from 67 wells in the study area, the aforementioned method was employed to interpret three evaluation parameters: mud content, porosity and permeability of the single layer. A comprehensive evaluation index R was introduced to quantitatively assess the sealing capacity of the single layer. Based on this study, there is a positive correlation between the sealing capacity of the single layer and the mud content, but a negative correlation with porosity and permeability. These three factors collectively influence sealing capacities, such that $|A_1|+|A_2|+|A_3| = 1$. A_1, A_2, and A_3 are assigned values of
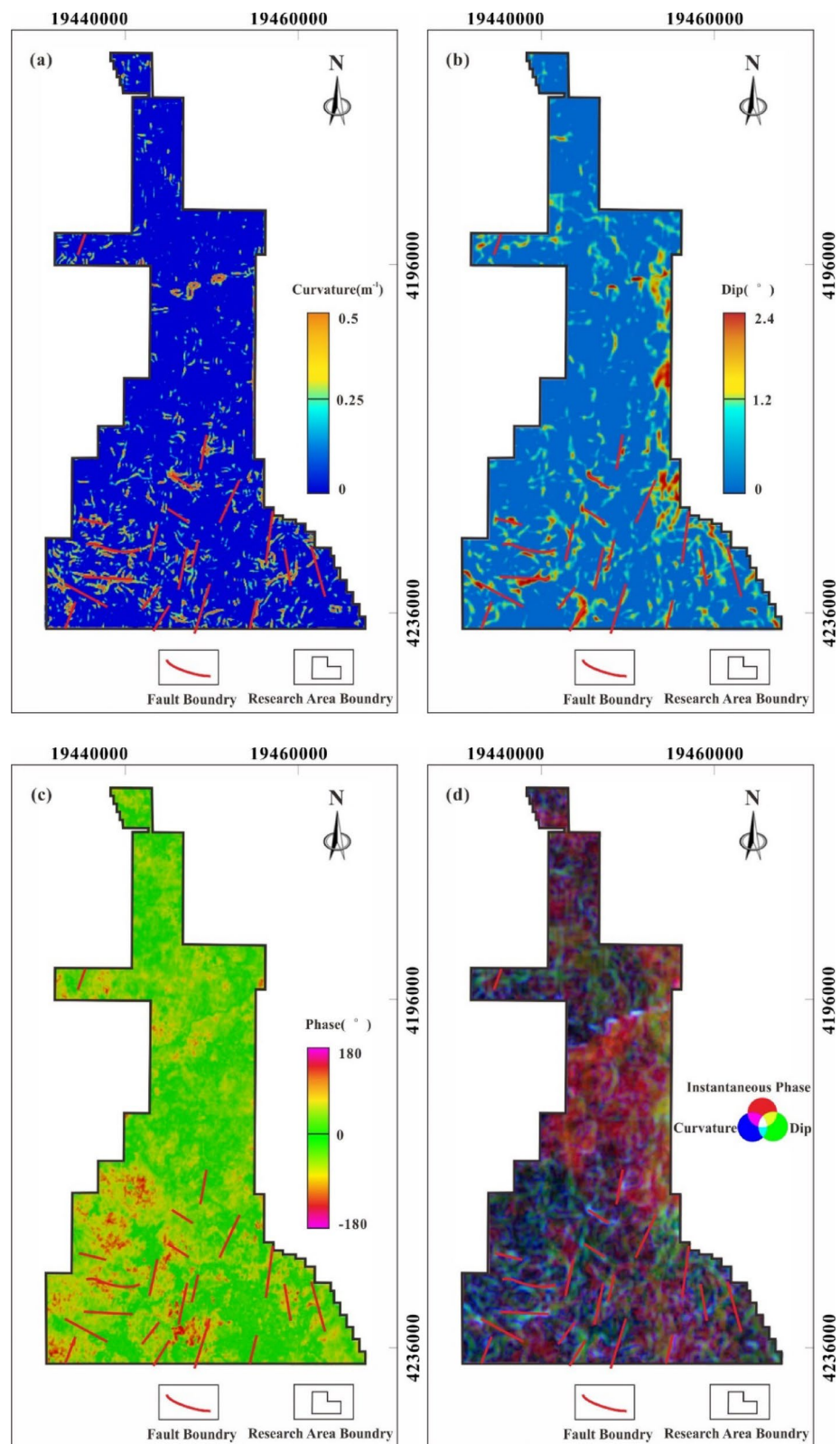
Fig. 8. Seismic attributes and their overlapping effect with faults. (**a**) Curvature (**b**) Dip (**c**) Instantaneous phase (**d**) Fused attribute by RGB fusion technology.
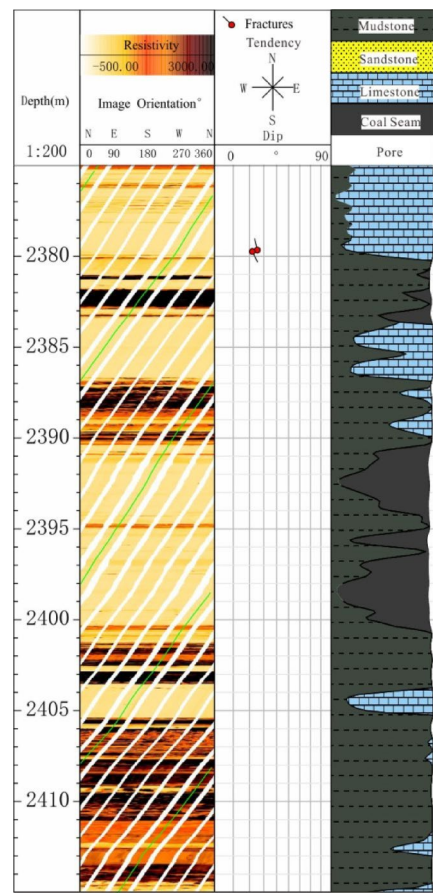
Fig. 9. Imaging logging of J33-3.

Well	Location	Depth (m)	Length (m)	Density (#/m)	Fused attribute
J33-3	Roof	2379.5–2380.0	2.06	2	0.00030
J34-2	None				0.00008
J36-5C3	Floor	2195.7–2201.6	1.64	2	0.00031
J37-2	None				0.00013
J44-3	None				0.00022
J47-4	None				0.00007
J53-2	None				0.00021
JN2	Floor	2415.6–2416.2	4.19	4	0.00051

Table 2. Fracture development characteristics interpreted by imaging logging and fused attribute at wells.

0.4, 0.3, and 0.3, respectively, according to geological principles[12]. Therefore, the quantitative calculation formula for the comprehensive evaluation index R for the sealing capacity of the single layer is defined as Eq. 9.

$$R = A_1 V_{sh} + A_2 \varphi + A_3 K \tag{9}$$

Where R is the sealing capacity index of the single layer; A_1, A_2, A_3 respectively stand for influence coefficients of V_{sh}, φ and K.

The ratio of mudstone thickness to formation thickness (M) within 15 m needs to be calculated. The calculation formula of M is shown as:

$$M = \frac{H_m}{15} \tag{10}$$

Where M is ratio of mudstone to formation; H_m is thickness of mudstone, m.

The influence of the single layer on the sealing capacity of CBM is related to its distance from the coal seam. The greater the distance between the single layer and the coal seam, the smaller the impact of the single layer on the sealing effect of CBM. Therefore, the distance index D is introduced to characterize the effect of the distance between the single layer and the coal seam on the sealing capacity of the single layer. The distance indices Dt and Db for the roof and floor are defined in Eq. 11.

$$D_t = \frac{|H - H_{ct}|}{15}$$
$$D_b = \frac{|H - H_{cb}|}{15}$$

(11)

Where D_t and D_b are distance indices of the roof and floor respectively; H is the elevation of the single layer, m. H_{ct} and H_{cb} are elevation of the top and bottom of the coal seam respectively, m.

The sealing capacity of the roof and floor within the 15 m range above and below the top and bottom of the No. 8 coal seam is defined as S. It is influenced by the sealing capacity of a single layer, the distance index, and the intensity of fracture development. Consequently, a quantitative formula for the sealing capacity of the roof and floor was derived.

$$S = \sum_{i}^{m} R_i \cdot D_i \cdot M \cdot F$$

(12)

Where S is sealing capacity index of roof and floor; the roof and floor are divided into m layers; i is the i-th layer; R_i is the sealing capacity of the i-th layer; D is distance indice of the i-th layer respectively.

The sealing capacities of the roof and floor were evaluated depending on the comprehensive evaluation index S, followed by normalization, as shown in Fig. 10. Figure 11 illustrates the distribution characteristics of the sealing capacities in the study area. The overall sealing capacities of the roof are good, with poor sealing capacities found only in a small portion of the central area. The overall sealing capacities of the floor are also good, although they are poor in the northwest and southeast sections.

Influences factors for sealing capacity

Pores, microfractures, and various forms of micro-permeable spaces provide channels for the escape of CBM when interconnected. The sealing mechanism of the roof and floor against gases is primarily due to the presence of permeability channels in sediments.

Sediments of different grain sizes create channels of varying dimensions and have differing sealing effects on gas. Mud content influences the pore structure in rocks, making it a critical factor in the sealing capacities of the roof and floor. Among the various lithologies in the study area, mudstone exhibits the best sealing capacity, while sandstone demonstrates the poorest sealing capacity.

Differences in rock physical properties can also lead to variations in sealing capacities, including porosity and permeability. Greater porosity results in more pore space within the rock, which increases the size of gas escape channels and thus makes effective gas sealing less likely. Additionally, the connectivity of the pores significantly influences sealing capacity. Permeability reflects the connectivity of the pore space; higher permeability allows fluids to pass through the rock more quickly, indicating that the pores are more interconnected and therefore less effective in terms of sealing capacity.

In addition to the pore space within the rock itself, later tectonic movements can create fractures in the strata, forming larger-scale gas flow channels that can affect the sealing capacity of the roof and floor[30,31]. Fractures in the roof and floor significantly impact their longitudinal permeability, allowing the transportation and diffusion of coalbed methane outward along these channels. The development of fractures is more pronounced in and
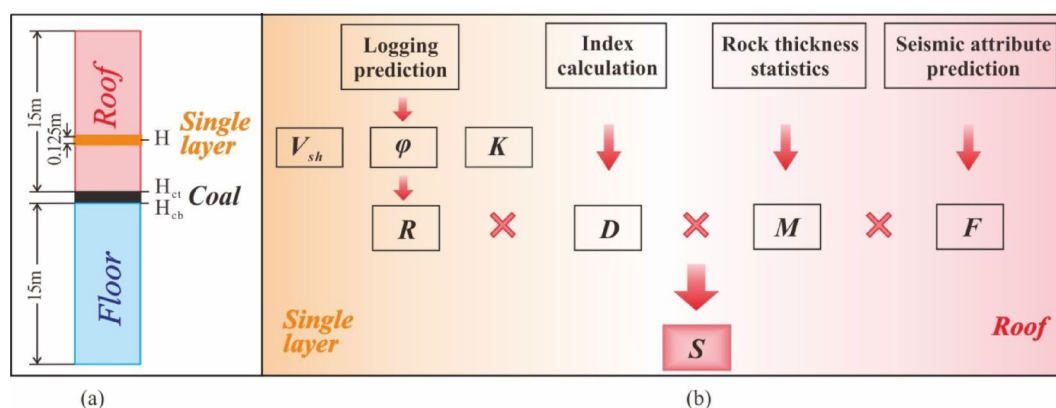
Fig. 10. (**a**) Sketch map of roof and floor. (**b**) The workflow chart of the sealing capacities of the roof and floor (taking the roof as an example).
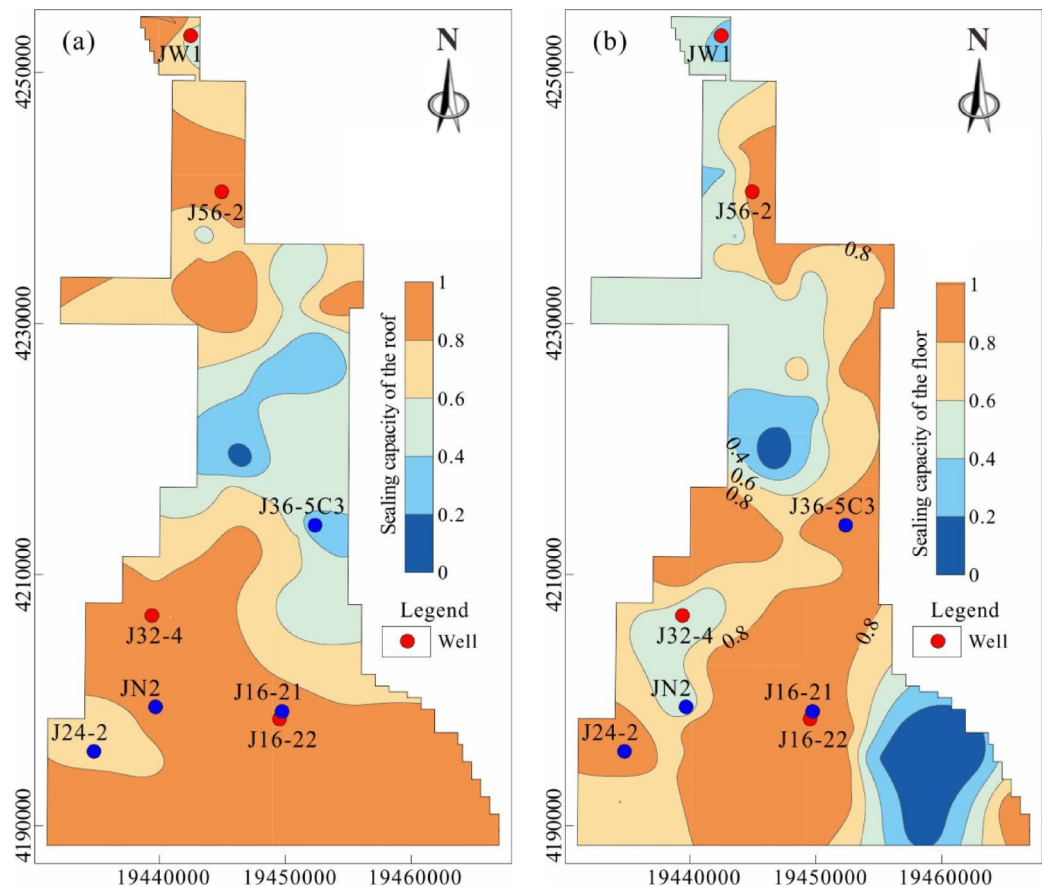
Fig. 11. (**a**) The sealing capacity of the roof. (**b**) The sealing capacity of the floor.

around tectonic zones such as faults and folds. The overall research area is characterized by gentle monocline tectonics, so the fractures are not significantly influenced by folds. Consequently, the degree of crack development in this research area is primarily related to faults. Faults not only affect the sealing capacities of the roof and floor at the fault locations but also influence the sealing capacities in the surrounding areas. Therefore, using 3D seismic data to predict the intensity of fracture development is effective.

In summary, five parameters that effectively reflect sealing capacity are selected: mud content, mudstone-to-formation ratio, porosity, permeability, and fracture development intensity.

Influence of sealing capacities of roof and floor on gas content

Four wells are undergoing core drilling while maintaining formation pressure, and four additional wells are engaged in wireline coring within the study area. The gas content of the No. 8 coal seam has been measured, with their locations illustrated in Fig. 11. A strong positive correlation has been identified between gas content and the sealing capacities of the roof; however, no significant correlation exists between gas content and the sealing capacities of the floor, as depicted in Fig. 12. It is understood that when free gas escapes upward, it becomes sealed by the roof. The lower the porosity and permeability of the roof, along with less developed fractures, the more conducive it is for the in situ preservation of free gas in the coal seam. Given the high proportion of free gas in deep coalbed methane (CBM)[32], stronger sealing capacities of the roof facilitate the preservation of free gas, leading to a higher total gas content in the coal seam. Conversely, the floor does not significantly influence this process.

Sealing pattern of roof and floor of coal seam

Differences in the physical properties of the roof and floor can lead to variations in their sealing capacities. The overall lithology of the roof and floor of Pattern A in M5 was mudstone, with an average mud content of 33.08% in the roof, a mudstone-to-formation ratio of 100%, an average porosity of 1.17%, an average permeability of 4.63 mD, and a fracture development intensity of 8.35% based on curvature attributes. The floor had an average mud content of 27.03%, a mudstone-to-formation ratio of 58%, an average porosity of 2.16%, an average permeability of 8.68 mD, and a fracture development intensity of 9.56%. The fractures in the roof and floor were not well developed, and the other parameters differed significantly from those of the coal seam, which had an average porosity of 2.28% and a permeability of 2.13 mD. This created a favorable sealing capacity for the roof and floor of Pattern A.
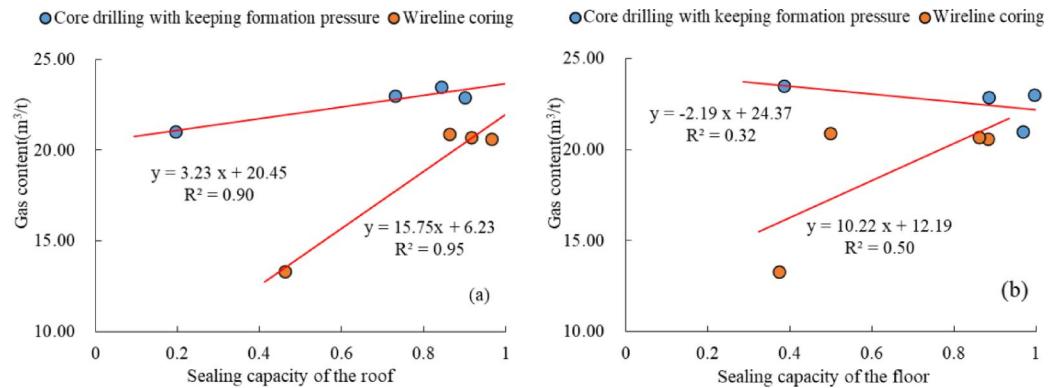
Fig. 12. (**a**) The correlation between gas content and the sealing capacity of the roof. (**b**) The correlation between gas content and the sealing capacity of the floor.

The roof and floor of Pattern B in J35-4 contained a certain thickness of sandstone, with an average mud content of 32.18%, a mudstone-to-formation ratio of 66.67%, an average porosity of 1.82%, an average permeability of 6.58 mD, and a fracture development intensity of 11.25%. The average mud content of the floor was 40.69%, mudstone-to-formation ratio was 82.67%, average porosity was 1.76%, average permeability was 6.31 mD, and fracture development intensity was 9.36%. The fractures in the roof and floor were not well developed, and the other parameters differed from those of the coal seam. The porosity and permeability of Pattern B's roof were higher than those of Pattern A, which gave the roof and floor of Pattern B a general sealing capacity.

The overall roof of Pattern C in M57 was sandstone, with an average mud content of 19.89%, a mudstone-to-formation ratio of 33.33%, an average porosity of 5.30%, an average permeability of 601.44 mD, and a fracture development intensity of 9.45%. The average mud content of the floor was 41.29%, mudstone-to-formation ratio was 82.00%, average porosity was 2.04%, average permeability was 7.81 mD, and fracture development intensity was 10.33%. The fractures in the roof and floor were not well developed, and the poor physical conditions of the roof resulted in a low sealing capacity for Pattern C.

The locations of M5, J35-4, and M57 are shown in Fig. 1. The analysis indicates that the sealing capacity of the roof and floor is associated with mud content, mudstone-to-formation ratio, porosity, permeability, and fracture development intensity. Data on the influencing parameters of the three patterns in M5, J35-4, and M57 were collected. Owing to the significant impact of the sealing capacity of the roof on deep CBM, the roof data were normalized, and a radar chart was created to analyze the impact of the five parameters on sealing capacity, providing a judgment chart for the classification of the sealing capacity modes (Fig. 13).

Sealing capabilities were divided into three patterns. The mud content and mudstone-to-formation ratio of the roof of Pattern A were high, while the porosity, permeability, and intensity of fracture development were low. Pattern A was located at the bottom of the radar chart and had a shape similar to that of a triangle. The mud content, mudstone-to-formation ratio, porosity, and permeability of the roof of Pattern B were all in the middle range. Pattern B was situated in the middle of the radar chart, with an irregular pentagon shape. The mud content and mudstone-to-formation ratio of the roof of Pattern C were low; however, the porosity and permeability were high. Pattern C was located in the upper part of the radar chart and had a shape similar to that of an inverted triangle.

When the fault did not develop and the organic matter maturity of the coal seam was similar, Patterns A and B created high-quality sealing combinations, facilitating the preservation of CBM in the coal seam. As a result, the coal seam had good gas content. However, Pattern C exhibited poor sealing performance, allowing free gas in the coal seam to migrate upward, leading to gas loss and ultimately resulting in low gas content in the coal seam.

Comparison between sealing capacity evaluation model and traditional model

In order to test the effectiveness of our sealing capacity evaluation model, we compared it with a currently widely used model. The traditional model uses logging data to quantitatively evaluate the sealing capacity of coal seam roof and floor. The model combines logging data and experimental data, and optimizes five parameters including mud content, rock thickness, porosity, permeability, and fracture index to construct a sealing capacity calculation model[33]. Applying the model to the study area and comparing the calculated results with our model, it was found that our model had better application performance, and the calculated sealing capacity of the roof by our model had a stronger correlation with the gas content tested by core drilling with keeping formation pressure, as shown in Fig. 14.

It was found that both models referenced many common influences factors through comparing the construction methods of two sealing capacity evaluation models. The traditional model simply takes the average of parameters within a certain thickness for subsequent calculation, but our model also considers the distance index more, which takes into account the influence of the distance between the strata and the coal seam on the sealing ability of the strata to CBM. Moreover, our model and traditional model have different prediction methods for jointly influences factors. For instance, we predict porosity and permeability based on lithology separately, which is a more reasonable prediction method. In addition, we predicted the fracture development
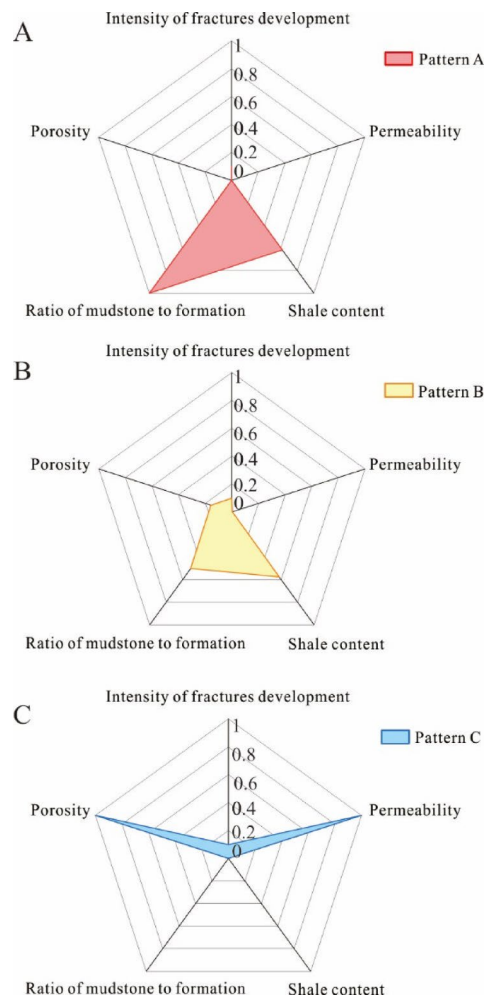
Fig. 13. Sealing evaluation parameters of the roof and floor of M5, J35-4 and M57. (**a**) Sealing evaluation parameters characteristics of Pattern (A). (**b**) Sealing evaluation parameters characteristics of Pattern (B). (**c**) Sealing evaluation parameters characteristics of Pattern C.
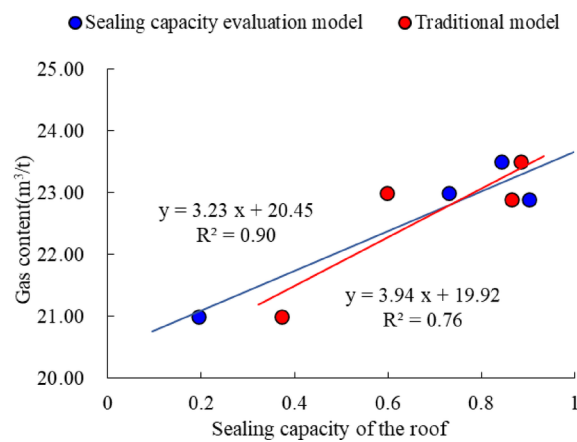
Fig. 14. The correlation between gas content and the sealing capacity of the roof predicted by different models.

intensity based on seismic data and combined with seismic attribute fusion technology. Compared with the method of logging prediction, our method has higher lateral resolution and better plane prediction effect.

Applicability of sealing capacity evaluation model

Our sealing capacity evaluation method is based on experimental data from the study area, therefore it has certain regional characteristics. If this method is applied to other regions, new prediction methods need to be constructed for the five sealing capacity influencing factors, which requires comprehensive data, such as porosity and permeability testing data, conventional logging data, imaging logging data, 3D seismic data, etc.

Specifically, a logging prediction model should be constructed using the porosity and permeability data in the region. Besides, the calculation of mud content also needs to consider the formation period of the studied strata. In addition, the fracture development intensity has regional characteristics especially, so it is necessary to utilize 3D seismic data for attribute optimization and fusion. Due to different fracture conditions in different regions, different attributes may be selected from this article, but attribute fusion can still be used to quantitatively evaluate the fracture development intensity. In summary, as long as experimental data, logging data, 3D seismic data, and other data from other regions are analyzed according to the research thought of this article, our method can be effectively applied to other regions.

Conclusions

Prediction models for five parameters were established, and a comprehensive sealing capacity evaluation model was constructed to quantitatively assess the sealing capacity of the roof and floor. Moreover, the influence of the roof and floor on deep CBM accumulation was analyzed. The following conclusions were drawn:

1. The sealing capacity of the roof and floor was influenced by five key factors: mud content, mudstone-to-formation ratio, porosity, permeability, and fracture development intensity. Prediction models for the physical properties of the roof and floor were developed based on the correlation between geophysical logging data and experimental data of these properties. Ultimately, a comprehensive evaluation model for the sealing capacity of the roof and floor was established.
2. The correlation between gas content and sealing capacity was analyzed, revealing a positive relationship between gas content and the sealing capacity of the roof. The higher the mud content and mudstone-to-formation ratio of the roof, the lower the porosity and permeability, and the less developed the fractures, resulting in a stronger sealing capacity of the roof, which is more conducive to the preservation of free gas in the coal seam. However, there was no significant correlation between gas content and the sealing capacity of the floor.
3. The sealing capacity was divided into three patterns from five aspects: mud content, mudstone-to-formation ratio, porosity, permeability, and fracture development intensity. Patterns A and B are considered high-quality sealing combinations, and the gas content in the coal seam was high. By contrast, Pattern C exhibited poor sealing performance, resulting in low gas content in the coal seam.

Data availability

The datasets used and/or analyzed in the current study are available from the corresponding author upon reasonable request.

References
1. Qin, Y., Shen, J. & Li, X. G. Control degree and reliability of CBM resources in China. *Nat. Gas. Ind.* **42**(6), 19–32 (2022). (In Chinese with English abstract).
2. Xu, F. Y. et al. Deep (layer) coalbed methane reservoir forming modes and key technical countermeasures-taking the Eastern margin of Ordos basin as an example. *China Offshore Oil Gas.* **34**(4), 30–42 (2022). (In Chinese with English abstract).
3. Pu, Y. F., Li, S., Tang, D. Z. & Chen, S. D. Effect of magmatic intrusion on in situ stress distribution in deep coal measure strata: A case study in Linxing block, Eastern margin of Ordos basin, China. *Nat. Resour. Res.* **5**, 2919–2942 (2022).
4. Li, G. Y. et al. Deep coalbed methane resources in the Shenmu-Jiaxian block, Ordos basin, China: geological characteristics and potential for exploration and exploitation. *Coal Geol. Explor.* **52**(2), 70–80 (2024). (In Chinese with English abstract).
5. Cai, Y. D., Liu, D. M., Yao, Y. B., Li, J. Q. & Qiu, Y. K. Geological controls on prediction of coalbed methane of 3 coal seam in Southern Qinshui basin, North China. *Int. J. Coal Geol.* **88**(2), 101–112 (2011).
6. Qin, Y., Tang, X. Y., Ye, J. P. & Jiao, S. H. Characteristics and origins of stable carbon isotope in coalbed methane of China. *J. China Univ. Min. Technol.* **29**(2), 113–119 (2000). (In Chinese with English abstract).
7. Liu, D. M. et al. A new insight into coalbed methane occurrence and accumulation in the Qinshui basin, China. *Gondwana Res.* **111**, 280–297 (2022).
8. Liu, D. M., Yao, Y. B. & Wang, H. Structural compartmentalization and its relationships with gas accumulation and gas production in the Zhengzhuang field, Southern Qinshui basin. *Int. J. Coal Geol.* **259**, 104055 (2022).
9. Su, X. B., Lin, X. Y., Zhao, M. G., Song, Y. & Liu, S. B. The upper paleozoic coalbed methane system in the Qinshui basin, China. *AAPG Bull.* **89**(1), 81–100 (2005).
10. Meng, Y. J. et al. Geological controls and coalbed methane production potential evaluation: A case study in Liulin area, Eastern Ordos basin, China. *J. Nat. Gas Sci. Eng.* **21**, 95–111 (2014).
11. Jin, K. et al. The effect of sedimentary redbeds on coalbed methane occurrence in the Xutuan and Zhaoji coal mines, Huaibei coalfield, China. *Int. J. Coal Geol.* **137**, 111–123 (2015).
12. Liu, Z. M., Han, W. L., Ni, D., Zhang, C. R. & Zhuang, D. Sealing research of coal seam roof and floor based on conventional logging data. *Coal Technol.* **37**(12), 100–103 (2018). (In Chinese with English abstract).
13. Tian, F. C., Liang, Y. T., Wang, D. M. & Jin, K. Effects of caprock sealing capacities on coalbed methane preservation: experimental investigation and case study. *J. Cent. South. Univ.* **26**(4), 925–937 (2019).
14. Yang, H., Xi, S. L., Wei, X. S. & Li, Z. H. Evolution and natural gas enrichment of multicycle superimposed basin in Ordos basin. *China Petroleum Explor.* (01), 17–24. (2006).

15. Liu, D. M., Zhao, Z., Cai, Y. D. & Sun, F. R. Characterizing coal gas reservoirs: A multiparametric evaluation based on geological and geophysical methods. *Gondwana Res.* **133**, 91–107 (2024).
16. Li, C. L. et al. Distribution law of occurrence state and content prediction of deep CBM: A case study in the Ordos basin, China. *Nat. Resour. Res.* **33**(4), 1843–1869 (2024).
17. Lai, J., Wang, G. W., Ran, Y., Zhou, Z. L. & Cui, Y. F. Impact of diagenesis on the reservoir quality of tight oil sandstones: the case of upper triassic Yanchang formation Chang 7 oil layers in Ordos basin, China. *J. Petrol. Sci. Eng.* **145**, 54–65 (2016).
18. Bitrus, R. P., Iacopini, D. & Bond, E. C. Defining the 3D geometry of thin shale units in the sleipner reservoir using seismic attributes. *Mar. Pet. Geol.* **78**, 405–425 (2016).
19. Li, L. F., Huang, Y. P. & Qi, X. M. Recognition of small faults in coal fields based on multi-scale seismic curvature attributes fusion. *Heliyon*, **9**(11) (2023).
20. Di, H. B. & Gao, D. L. 3D seismic flexure analysis for subsurface fault detection and fracture characterization. *Pure. Appl. Geophys.* **174**, 747–761 (2017).
21. Hamidi, R., Ghosh, D. & Bashir, Y. A new approach to fractured damage zone evaluation using wavelet transform and variance attribute, EAGE conference on reservoir geoscience. *Eur. Assoc. Geosci. Eng.* **2018**(1), 1–5. (2018).
22. Zhang, X. X., Yu, J. J., Li, N. Y. & Wang, C. Multi-scale fracture prediction and characterization method of a fractured carbonate reservoir. *J. Petroleum Explor. Prod. Technol.* **11**(1), 1–12 (2020).
23. Ashraf, U. et al. Controls on reservoir heterogeneity of a shallow-marine reservoir in Sawan gas field, SE Pakistan: implications for reservoir quality prediction using acoustic impedance inversion. *Water* **12**(11), 2972 (2020).
24. Bai, B., Yang, C. & Sun, W. B. Simultaneously computing the 3D dip attributes for all the time samples of a seismic trace. *J. Geophys. Eng.* **18**, 691–699 (2021).
25. Abbas, A., Zhu, H. T., Anees, A., Ashraf, U. & Akhtar, N. Integrated seismic interpretation, 2D modeling along with petrophysical and seismic attribute analysis to Decipher the hydrocarbon potential of Missakeswal area. *Pakistan J. Geol. Geophys.* **8**(1), 1–12 (2019).
26. Mohammadi, R. & Bakhtiari, M. R. Faults and fractures detection using a combination of seismic attributes by the MLP and UVQ artificial neural networks in an Iranian oilfield. *Pet. Sci. Technol.* **41**(24), 2299–2327 (2023).
27. Chen, G. Q., Wang, B. X., Liu, M. & Liu, G. W. Linear projection decolorization algorithm based on structural information similarity. *J. Jilin Univ. (Science Edition)*. **58**(04), 877–884 (2020). (In Chinese with English abstract).
28. Lai, J. et al. A review on the applications of image logs in structural analysis and sedimentary characterization. *Mar. Pet. Geol.* **95**, 139–166 (2018).
29. Fernández Ibáñez, F., DeGraff, J. M. & Ibrayev, F. Integrating borehole image logs with core: A method to enhance subsurface fracture characterization. *AAPG Bull.* **102**(6), 1067–1090 (2018).
30. Yao, Y. B. et al. Preliminary evaluation of the coalbed methane production potential and its geological controls in the Weibei coalfield, southeastern Ordos basin, China. *Int. J. Coal Geol.* **78**(1), 1–15 (2008).
31. Yao, Y. B., Liu, D. M. & Yan, T. T. Geological and hydrogeological controls on the accumulation of coalbed methane in the Weibei field, southeastern Ordos basin. *Int. J. Coal Geol.*, 148–159 (2014).
32. Yao, Y. B., Wang, F., Liu, D. M., Sun, X. X. & Wang, H. Quantitative characterization of the evolution of in-situ adsorption/free gas in deep coal seams: insights from NMR fluid detection and geological time simulations. *Int. J. Coal Geol.* **285**, 104474 (2024).
33. Liu, Z. D. et al. Quantitatively evaluating sealing ability of coal roof and floor using logging data. *J. Cent. South. Univ. (Science Technology)*. **46**(03), 1100–1109 (2015). (In Chinese with English abstract).

Acknowledgements

Author contributions

Q.Z.: Writing – original draft, Investigation, Formal analysis; P.L.: Methodology, Data support; D.L.: Writing – review & editing, Conceptualization, Methodology, Funding acquisition; Y.Y.: Writing – review & editing, Methodology, Visualization, Funding acquisition; Y.C.: Methodology; Y.G.: Methodology, Technical assistance; Z. W.: Methodology, Technical assistance.

Declarations

Competing interests

The authors declare no competing interests.

Additional information

Correspondence and requests for materials should be addressed to D.L.

Reprints and permissions information is available at www.nature.com/reprints.

Publisher's note Springer Nature remains neutral with regard to jurisdictional claims in published maps and institutional affiliations.